


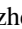


Strain-enhanced spin-orbit coupling in permalloy thin filmsSicong Hu ^{1,*}, Er Liu ^{1,*,\dagger}, Yuqing Bai ¹, Mingzhe Zhuang,¹ Wenwen Liu,¹ Mingyue Lei,¹ Yujing Zhang,¹ Guizhou Xu,¹ Feng Xu ^{1,\ddagger} and Stéphane Mangin²¹*MIT Key Laboratory of Advanced Metallic and Intermetallic Materials Technology, School of Materials Science and Engineering, Nanjing University of Science and Technology, Nanjing 210094, China*²*Université de Lorraine, CNRS UMR 7198, Institut Jean Lamour, F-54011 Nancy, France*

(Received 10 November 2023; revised 22 April 2024; accepted 13 May 2024; published 4 June 2024)

A comprehensive analysis of the impact of strain on spin-orbit coupling (SOC) in permalloy (Py, Ni₈₀Fe₂₀) thin films is presented. Utilizing a combination of ferromagnetic resonance (FMR) and x-ray magnetic circular dichroism (XMCD) techniques, we systematically evaluate the modifications in SOC as a function of applied strain. Our FMR data indicate a marked enhancement in Gilbert damping and an increase in the perpendicular magnetic anisotropy constant, suggesting that SOC strength intensifies with both compressive and tensile strains. XMCD results, in concert with first-principles calculations, elucidate the underlying mechanism: strain-induced lattice distortions substantially elevate the orbital moments within the Py films. This boost in the orbital moment is attributed to the strain's modulation of the orbital quenching effect, revealing a direct correlation between lattice strain and SOC enhancement. These insights not only deepen our understanding of SOC in ferromagnetic thin films but also have potential implications for the design of spintronic devices where controlling SOC is paramount.

DOI: [10.1103/PhysRevB.109.224407](https://doi.org/10.1103/PhysRevB.109.224407)**I. INTRODUCTION**

Spin-orbit coupling (SOC) describes the interplay between electronic spin and orbit degrees of freedom—a relativistic effect which can be regarded as an effective magnetic field experienced by the spin of an electron in the rest frame [1,2]. Since SOC connects the spin of the electron and its orbit, in condensed matter, SOC is sensitive to the lattice and the band structures, thereby playing a fundamental role in rich phenomena [3], from magnetic anisotropy, the anomalous Hall effect (AHE), and anisotropic magnetoresistance (AMR) which were observed centuries ago, to the recently discovered spin Hall effect in heavy metals [4] and topological insulators [5,6], etc. Many of the above phenomena are pivotal to several technical revolutions in the fields of magnetic sensors and magnetic storage. As such, SOC has been the center of magnetism and spintronics since it emerged a century ago [7,8], and effective approaches to manipulate SOC in magnetic materials are urgently needed. Previous efforts focused on the introduction of elements with large atomic numbers, such as a combination of a heavy metal (HM) with a thin ferromagnet (FM) to drive a stronger SOC at the HM/FM interface [9,10] and doping of heavy elements in ferromagnet or ferromagnetic semiconductors [11,12], etc.

In this paper, we report an alternate approach to enhance SOC in pure permalloy thin films without any doped or adjacent heavy element, via tailoring the Py lattice with uniaxial

strain introduced by a flexible substrate. The Py films, which have a negligible magnetostriction constant, were deposited on flexible mica substrates, and the strain was induced by placing the substrates on concave or convex aluminum molds during the deposition. The influence of strain on the SOC of Py films has been systematically investigated by ferromagnetic resonance (FMR) and x-ray magnetic circular dichroism (XMCD) studies. The amplitude of SOC is then evaluated by the extracted magnetic damping and perpendicular magnetic anisotropy from the FMR measurements, as well as by the calculated ratio of orbit to spin moment from the XMCD analysis. All experiments show a consistent result; that is, the introduced strains, whether they are compressive or tensile, both enhance the SOC in Py films. The demonstrated results shed further insight into the interplay between SOC and related observable phenomena. Further research based on these findings could open new avenues for tailoring and optimizing thin film properties for specific technological purposes.

II. EXPERIMENT

Samples with the structure of Cu (5)/Py (10)/Al (2) (all thicknesses in nm) were deposited on flexible Mica (AlF₂O₁₀Si₃₃Mg) substrates, which have a monoclinic lamellar crystalline form with relatively weak van der Waals bonding between each layer, and thus can be easily exfoliated along the (001) crystal plane.

The magnetic films were deposited at room temperature by magnetron sputtering using a Py (Ni₈₀Fe₂₀) target at a base pressure of 8×10^{-8} Torr and Ar pressure of 2×10^{-3} Torr. The deposition rate was about 1.5 Å/s, and a layer of Al (2 nm) was used to protect the surface. In our experiments, no

*These authors contributed equally to this work.

[†]ericliu@njust.edu.cn[‡]xufeng@njust.edu.cn

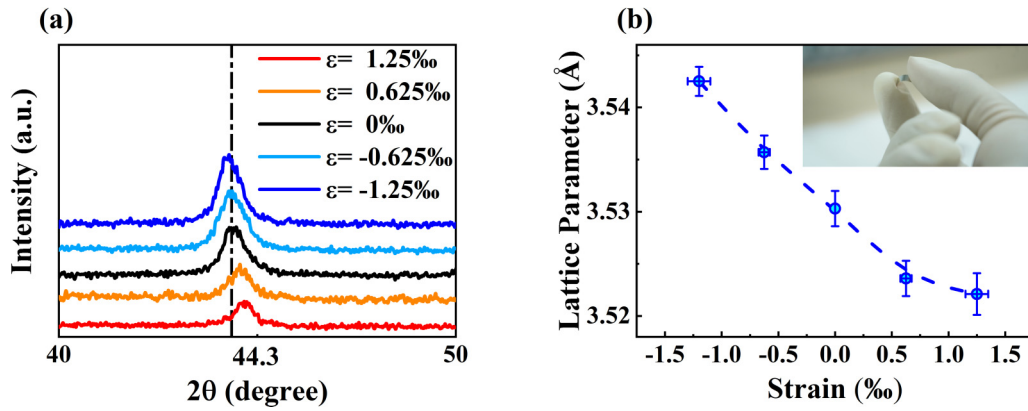


FIG. 1. (a) X-ray diffraction patterns of the main broad (111) peak of Cu (5)/Py (10)/Al (2) films with different strains. (b) The lattice parameter normal to the film as a function of strain. The inset shows a photo of a thin Cu/Py/Al film deposited on the flexible mica substrate.

magnetic field was applied during the deposition to minimize the parasitic effects of uniaxial anisotropy. Cu and Al layers were respectively chosen as the buffer and capping layers due to their negligible SOC and long spin diffusion length [13]. During the deposition, the flexible substrates were bent and fixed on homemade convex or concave aluminum semicylinder molds with different curvature radii. Compressive and tensile strains with different magnitudes can thus be induced in the Py films when the substrates were flattened after the deposition, and the induced uniaxial strain can be estimated by the equation below [14,15]:

$$\varepsilon = \frac{T}{2r}, \quad (1)$$

where ε is the in-plane compressive or tensile strain, r is the curvature radii of the mold, and T is the total thickness including both substrate and film. In the experiment, different mold curvature radii r of 10, 20, and 30 mm were employed to induce three strain magnitudes of 1.25%, 0.625%, and 0.416% [calculated using Eq. (1)], given that the thicknesses of substrates and films are 25 μm and 10 nm, respectively.

Within the FMR measurement process, the samples were placed facing downward on a coplanar waveguide (CPW) and subjected to the influence of a microwave field, denoted as h , with a frequency f ranging 8–17 GHz. In-plane magnetic fields H , ranging 0–3000 Oe, were applied perpendicular to h on the Py films. The FMR spectra were obtained by recording the relative magnetization as a function of H . X-ray magnetic circular dichroism (XMCD) measurements were used to determine the orbit and spin moments of the Py thin films under different strains. XMCD is a well-established element-specific technique for characterizing properties of material magnetism. Orbitals and spin moments can be obtained separately at each atomic site using a summation rule, especially in the case of the $L_{2,3}$ absorption edges of the Ni and Fe elements [16,17].

III. RESULTS AND DISCUSSION

A. Structure

Figure 1(a) shows x-ray diffraction patterns of the Py thin films in different strain states. The diffraction patterns for the sputtered films have a main broad peak at around 44.3° ,

corresponding to the $\text{Ni}_{80}\text{Fe}_{20}$ face-centered-cubic (111) plane. It is notable that the (111) peak shifts to high diffraction angles during the transition from compressive state to tensile state. This shifting indicates that the lattice constant of Py films increases with compressive strain while it decreases with tensile strain, as shown in Fig. 1(b). The result is reasonable as the strains were applied in plane on the Py thin films, thus the lattice parameters normal to the films would be increased (decreased) by the compressive (tensile) strain due to the constant film volume. A picture of the Py thin film deposited on a Mica substrate is shown in the inset of Fig. 1(b), manifesting good flexibility.

B. FMR measurements

1. Resonance fields

Figure 2(a) shows the FMR spectra excited at 13 GHz for the Py thin films with 0, +1.25%, and -1.25% strain. In the rest of the paper, we will use the plus and minus signs to denote tensile and compressive strain, respectively. It is interesting to note that, regardless of the type of applied strain, the resonance fields of compressive and tensile strained films both shift towards higher field directions. The shifting of resonance fields generally indicates a change of anisotropy in the magnetic film. However, permalloy is a well-known soft magnetic material with zero magnetostriction, thus the strain-induced in-plane magnetic anisotropy should be neglected. In fact, the in-plane angular dependent FMR measurements confirm the negligible in-plane anisotropy in our Py films, as shown in Fig. 2(b), in which isotropic shifting of resonance fields to the high field directions for the strained Py films can be well noted. To figure out the origin of the shifted resonance field in the strained Py films, we performed frequency-dependent FMR measurements, as shown in Fig. 2(c). The frequencies f dependent resonance fields H_{res} for all the Py films are obtained, which can be well fitted by the Kittel formula:

$$f = \left(\frac{\gamma}{2\pi}\right) [H_{\text{res}} (H_{\text{res}} + 4\pi M_{\text{eff}})]^{1/2}, \quad (2)$$

where γ is the gyromagnetic ratio, $M_{\text{eff}} = M_s - H_K^\perp$ is the effective magnetization, and M_s and H_K^\perp are the saturation magnetization and the perpendicular magnetic anisotropy

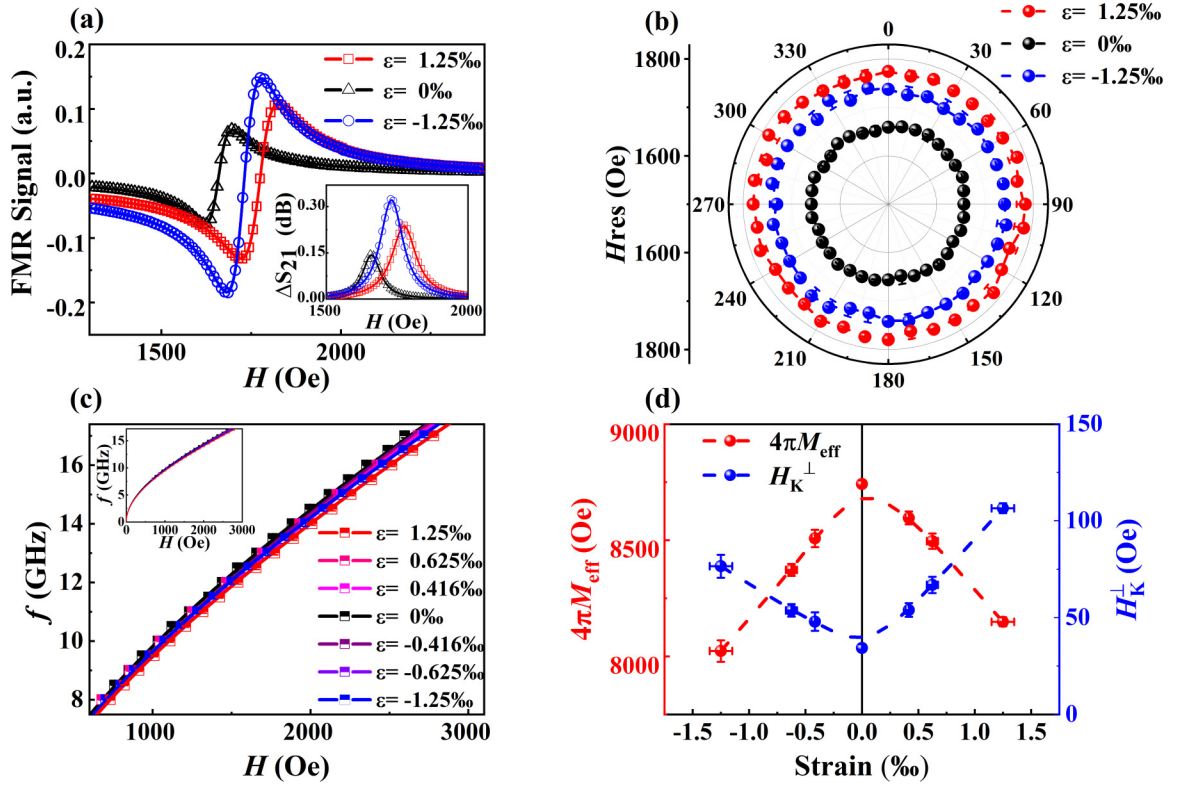


FIG. 2. (a) FMR spectra at 13 GHz for the Py films with different strains, the inset shows the microwave absorption spectrum. (b) In-plane angular dependence of H_{res} for the Py films with different strains. (c) Measured FMR frequency f as a function of H_{res} for the Py films. (d) The extracted values of $4\pi M_{\text{eff}}$ and H_{K}^{\perp} using Eq. (2) as a function of the applied strain.

field, respectively. Here we neglect the in-plane anisotropy field due to the negligible magnetostriction of Py films and use an empiric value of $\gamma/2\pi = 28.5$ GHz/T for the fitting process. Given the vibrating-sample magnetometer measured value of M_{s} (around 730 emu/cm³), the value of M_{eff} and H_{K}^{\perp} for all the films can be extracted from the fitting, as shown in Fig. 2(d). Notably, M_{eff} decreases with increasing strain (compressive and tensile), which gives rise to an increased H_{K}^{\perp} as well as a shifting of resonance fields in the strained Py films.

2. Resonance linewidth and damping

In addition to the resonance field, the resonance linewidths ΔH are also increased in the strained Py films, as shown in the inset of Fig. 2(a). The Gilbert damping α of the Py films can be obtained from the frequency dependence of the FMR linewidth using the equation [18]

$$\Delta H = \Delta H_0 + \frac{4\pi\alpha}{\gamma} f, \quad (3)$$

where ΔH_0 is the inhomogeneous broadening. Here we neglect the contribution of two-magnon scattering in the above equation due to the good linear relationship between the linewidth ΔH and frequency f [19]. The fitted curves agree well with the experimental results, as shown in Fig. 3(a). The strain dependence of Gilbert damping in the Py films can thus be obtained, as shown in Fig. 3(b). The obtained value of Gilbert damping α (0.0077) for our Py film with

$\varepsilon = 0$ is close to the value of Py film grown on a Si substrate [20], and it demonstrates similar dependence on the strain as that of perpendicular anisotropy H_{K}^{\perp} , i.e., increases with both compressive and tensile strain. The Gilbert damping increases to 0.0098 for the -1.25% strained film and 0.0107 for the $+1.25\%$ strained film. Moreover, the in-plane angular dependencies of α for the Py films with a strain of 0, $+1.25\%$, and -1.25% are also illustrated in Fig. 3(c), which show isotropic behavior for all the Py films, similar to that of resonance fields.

3. Discussion

The observed H_{K}^{\perp} and α increase as a function of strain may indicate an increase of SOC interaction in the Py films since both perpendicular anisotropy field H_{K}^{\perp} and Gilbert damping α are closely linked to SOC. In fact, the SOC constant (ξ_{SO}) can be calculated from the obtained value of H_{K}^{\perp} by fitting the resulting anisotropic energy densities using Bruno's theory [21]:

$$K = -\left(A \frac{N}{4V}\right) \frac{\xi_{\text{SO}}(\mu_{\text{L}}^{\perp} - \mu_{\text{L}}^{\parallel})}{\mu_{\text{B}}}. \quad (4)$$

K is the anisotropy energy density that can be obtained from $H_{\text{K}}^{\perp} = 2K/\mu_0 M_{\text{s}}$. A is a prefactor which depends on the electronic structure and varies between 0 and 0.2 [22], and a fixed value of $A = 0.1$ for all the Py films was used in our calculations [23]. N and V stand for the number of atoms per unit cell and the volume of the unit cell, respectively. Since the uniaxial strain does not change the volume of the lattice cell,

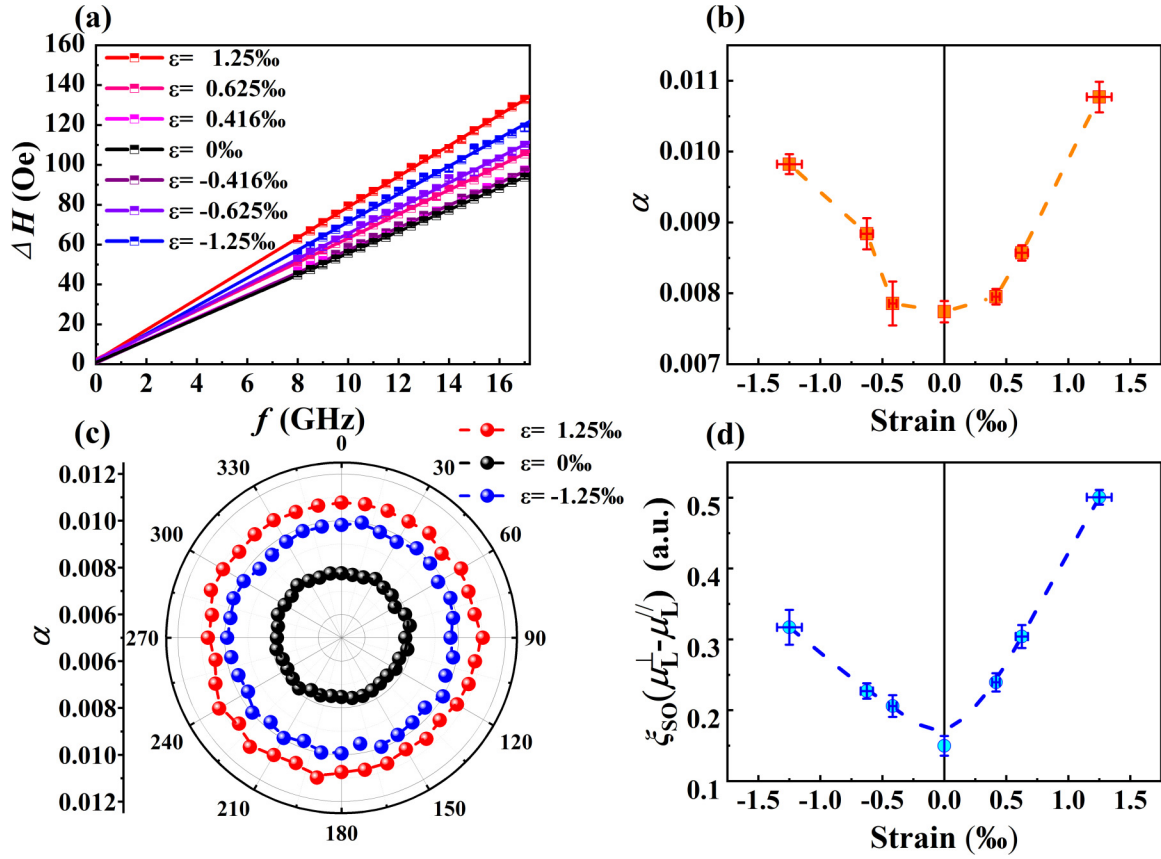


FIG. 3. (a) Frequency dependencies of linewidths (ΔH) for the Py films with different strains. (b) The extracted Gilbert damping as a function of the applied strain. (c) In-plane angular dependence of Gilbert damping for the Py films with different strains. (d) The obtained spin-orbit term as a function of strain.

we utilize constant values of $V = 4.474 \times 10^{-29} \text{ m}^3$ and $N = 4$ in the calculations. The SOC-related term $\xi_{SO}(\mu_L^\perp - \mu_L^\parallel)$ can be obtained from Eq. (4) and its strain dependence is shown in Fig. 3(d). We note that the obtained SOC-related term increases significantly with both the tensile and compressive strain.

C. Physical origin

1. Ab initio calculations

To unveil the physical origin of the observed strain-enhanced SOC, we performed a first principles calculation to evaluate the strain effect on the magnetic moments and density of states near the Fermi level $N(E_{F\pm})$ of Py. For simplicity, we considered strain in the films as a change in the lattice constant ($0, \pm 1.25\%$) of Py. The density function theory calculations were performed using the Vienna *ab initio* simulation package (VASP) [24,25]. The exchange-correlation effect was addressed using the Perdew-Burke-Ernzerhof (PBE) parametrization of the generalized gradient approximation (GGA) function [26], coupled with projector augmented wave (PAW) potentials [27]. The static self-consistency calculations were carried out on a k grid of $9 \times 9 \times 9$, with the cutoff energy of 500 eV for the plane wave basis set.

The calculated μ_S of both Fe and Ni keep constant when the strains are applied, as shown in Figs. 4(a) and 4(b). In contrast, the μ_L of both Fe and Ni increase significantly for

the strained Py lattice, giving rise to an enhanced orbital-to-spin moment ratio (μ_L/μ_S). Figure 4(c) shows the calculated values of the total μ_L/μ_S for the Py lattice with different strain states. The small ratio μ_L/μ_S of the unstrained Py lattice is noted, which can be ascribed to the lattice field induced orbital-quenching effect. The ratio μ_L/μ_S rises significantly for both compressive and tensile configurations, in agreement with the strain dependencies of H_K^\perp and α . The strain-enhanced μ_L/μ_S , which accounts for the strain-enhanced SOC, can be interpreted as the modified orbital quenching effect due to the strain-induced lattice distortion in the Py films [28]. However, it is important to underline that in addition to SOC, $N(E_{F\pm})$ is another factor affecting the Gilbert damping α as predicted by Kamberský's torque correlation model [29]:

$$\alpha \propto \left\langle \sum_{m,n} \left| \Gamma_{mk,nk}^- \right|^2 W_{mk,nk} \right\rangle_k. \quad (5)$$

The matrix element $\Gamma_{mk,nk}^-$, which measures the transitions between states in bands n and m induced by the spin-orbit torque, is proportional to the SOC in magnetic materials. The second term, $W_{mk,nk}$, denotes the electronic spectral overlap function of Bloch state lifetime, which is sensitive to the $N(E_{F\pm})$. We also calculated the $N(E_{F\pm})$ of the Py with different strain configurations to further clarify different

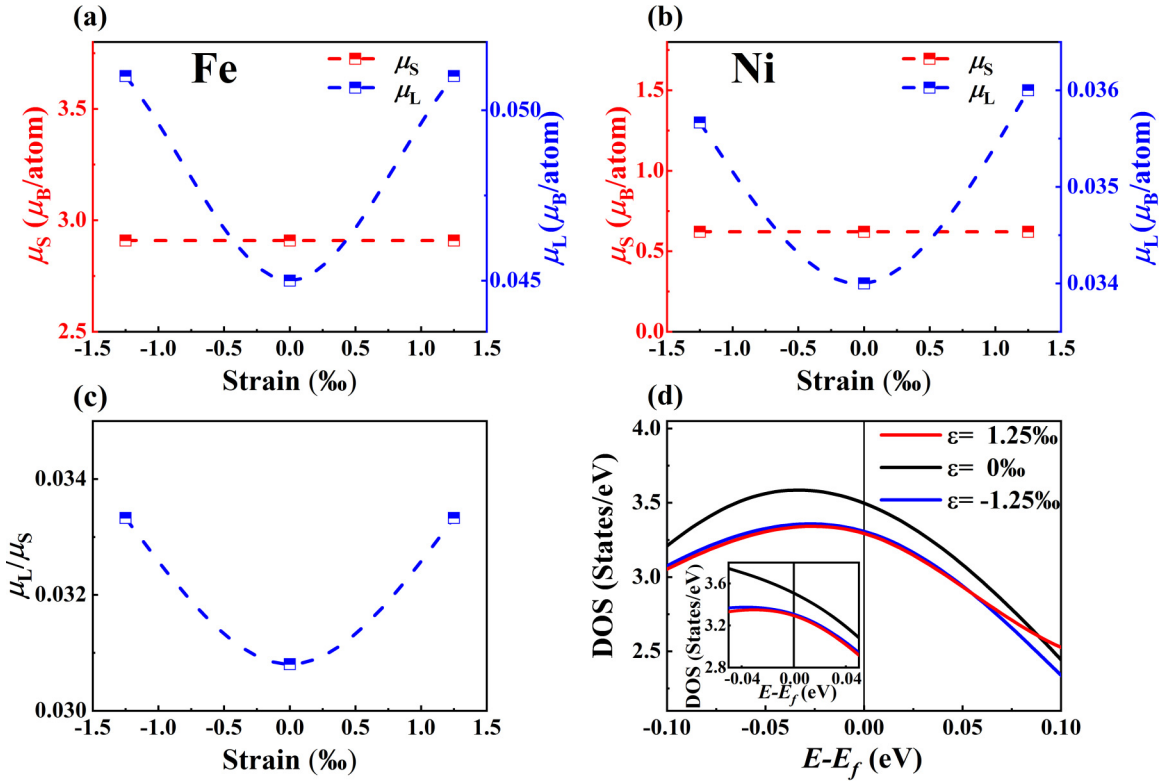


FIG. 4. Calculated variation of μ_L and μ_S of different elements in Py films with different strains: (a) Fe, (b) Ni. (c) Calculated variation of total μ_L/μ_S of Ni and Fe elements in Py films with different strains. (d) The total DOS near the Fermi level for the films with different strains, the inset shows an enlarged DOS near the Fermi surface.

contributions to the strain-enhanced α , as shown in Fig. 4(d). It is notable that the $N(E_F \pm)$ of Py decreases with both compressive and tensile strain, in stark contrast with the observed damping behavior. Therefore, we can safely ascribe the increase of Gilbert damping to the strain-enhanced SOC. The lattice constant used in the *ab initio* calculations is 3.55 Å; during strain application, the cell volume has been assumed to be constant and the magnitude of applied compressive and tensile strains on the lattice are the same as the magnitude used in the experiment.

2. XMCD measurements

To further confirm the above theoretical prediction, XMCD measurements on the Py films with different strains were also performed, which enable us to extract and separate the orbital and spin moments for each constituent element in the compound films [30]. The thin film samples were measured in total-electron-yield mode, with a fixed helicity of 80% circularly polarized x rays, and the MCD data were taken by alternating between two opposite directions of a saturation electromagnetic field (held at ~ 500 Oe) at each photon energy. The angle between the x rays and the film normal is 60° , and the magnetic field is parallel to the direction of the x rays.

In Figs. 5(b) and 5(c), μ^+ and μ^- refer to the absorption spectra when the magnetic field is parallel and antiparallel to the projection of the photon helicity on the sample plane, respectively. The XMCD spectral lines can be obtained from $\mu^+ - \mu^-$. P is the integral of the XMCD spectrum on the L_3

side, and q is the integral of the XMCD spectra on the $L_{2,3}$ sides. According to the summation rule, the orbital magnetic moment μ_L and the spin magnetic moment μ_S can be obtained from the following equations [31]:

$$\mu_L = -\frac{4}{3P} \frac{\int_{L_3+L_2} (\mu^- - \mu^+) dE}{\int_{L_3+L_2} (\mu^- + \mu^+) dE} (10 - n_{3d}), \quad (6)$$

$$\mu_S = -\frac{1}{P} \frac{6 \int_{L_3} (\mu^- - \mu^+) dE - 4 \int_{L_3+L_2} (\mu^- - \mu^+) dE}{\int_{L_3+L_2} (\mu^- + \mu^+) dE} \times (10 - n_{3d}) \left(1 + \frac{7 \langle T_z \rangle}{2 \langle S_z \rangle} \right)^{-1}, \quad (7)$$

where P is the x-ray circular polarization rate, n_{3d} is the $3d$ electron occupation number of the specific transition metal atom, $\langle T_z \rangle$ is the expectation value of the magnetic dipole operator, and $\langle S_z \rangle$ is equal to half of μ_S in Hartree atomic units. $\langle T_z \rangle / \langle S_z \rangle$ is expected to vary with the incidence angles. In our case, the angle of the incident x rays is 60° , which is close to the magic angle ($\sim 55^\circ$), thus the contribution of $\langle T_z \rangle / \langle S_z \rangle$ can be neglected [32]. The orbital-to-spin moment ratio μ_L/μ_S can therefore be expressed as

$$\mu_L/\mu_S = \frac{q}{3(1.5p - q)}. \quad (8)$$

Figure 5(d) shows the calculated μ_L/μ_S of Ni and Fe elements in films with different strains, and it can be found that the μ_L/μ_S of Ni and Fe elements follow the same dependence on the strain: they both increase due to the applied

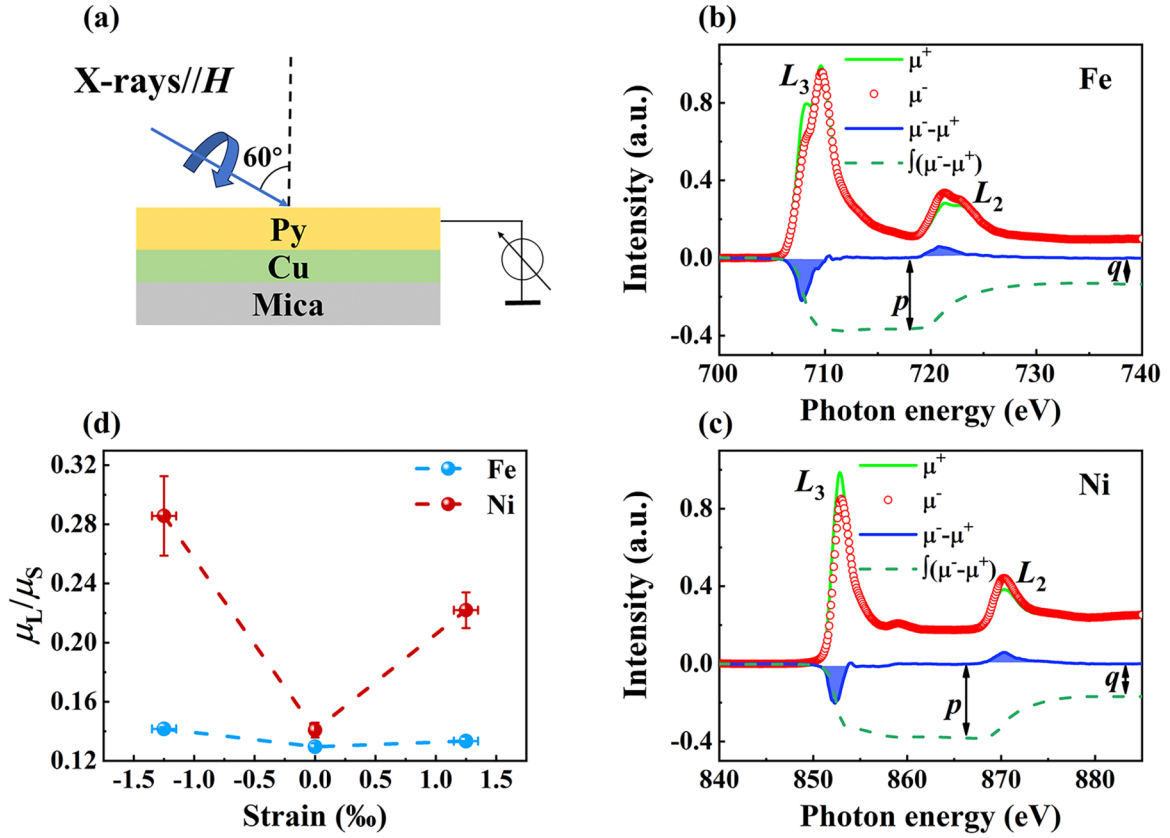


FIG. 5. (a) Schematic diagram of the experimental geometry for XMCD measurements under a magnetic field applied along the x-ray incidence direction and a grazing incidence (GI = 60°) of the x-ray beam. (b), (c) Typical x-ray absorption (XAS) and XMCD spectra at the Fe and Ni $L_{2,3}$ edges, respectively, of the unstrained permalloy films taken at room temperature. Integrals of the XMCD (dashed lines) are also shown. (d) Orbital-to-spin moment ratio (μ_L/μ_S) of Fe and Ni with different strains of 0, 1.25%, and -1.25% obtained from the XMCD spectra.

compressive and tensile strain, in line with the calculated results as shown in Fig. 4(c). The obtained μ_L/μ_S ratios of Ni and Fe for the strain-free sample are 0.14 ± 0.01 and 0.13 ± 0.01 , respectively, which are close to the reported values of 0.13 ± 0.03 for Ni and 0.10 ± 0.02 for Fe [33]. We also note that the increase of μ_L/μ_S due to compressive strain is larger than that induced by tensile strain, which may be due to the larger in-plane magnetic moment component [30] in the compressive strained Py film as it has smaller perpendicular anisotropy compared with tensile strained film [Fig. 2(d)]. Nevertheless, the demonstrated direct experiment evidence and theoretical calculations both verify a strain-induced increase of μ_L/μ_S , which gives rise to the enhanced SOC in the Py films.

It is noteworthy that the values of μ_L/μ_S obtained from *ab initio* calculations are significantly smaller than those extracted from XMCD analysis. In the *ab initio* calculations, for simplicity, we consider Py as a single crystal bulk material with infinite lattice periodicity. It has been experimentally reported that the orbital magnetic moments in thin films and nanoclusters with weak lattice periodicity can be strongly enhanced compared to those in their bulk counterparts [34,35]. In addition, the *ab initio* calculated value of μ_L/μ_S can be significantly underestimated as compared to the value extracted from XMCD analysis [36,37]. The above reasons may account for the large discrepancy between our *ab initio* calculation

and XMCD analysis on the value of μ_L/μ_S , although the two methods give similar strain dependencies of μ_L/μ_S in the Py.

D. Lande g factor

Since the accurate values of μ_L/μ_S ratios are obtained from XMCD measurements for our Py thin films with different strains, we can now evaluate the Lande g factor and its influence on our fittings. For small orbital contributions, the g factor can be expressed as [38]

$$g = 2 \left(\frac{\mu_L}{\mu_S} + 1 \right). \quad (9)$$

This formula can be extended to alloys and compounds, and the effective g factor g_{eff} in the case of Py reads [38]

$$g_{\text{eff}} = (0.8M_{\text{Ni}} + 0.2M_{\text{Fe}}) / \left(\frac{M_{\text{Ni}}}{g_{\text{Ni}}} + \frac{M_{\text{Fe}}}{g_{\text{Fe}}} \right), \quad (10)$$

where g_{Ni} and g_{Fe} are the g factors of Ni and Fe obtained by Eq. (9), and $M_{\text{Ni}} = 0.69 \mu_B$ and $M_{\text{Fe}} = 2.28 \mu_B$ are the magnetizations per atom of Ni and Fe [39]. Furthermore, the gyromagnetic ratio γ can be calculated as $\gamma = g_{\text{eff}}e/2m$, where e and m are the electron charge and mass. The obtained values of g_{eff} and γ are increased in the strained Py films, as shown in Fig. 6(a). We note that the value of γ of Py film at

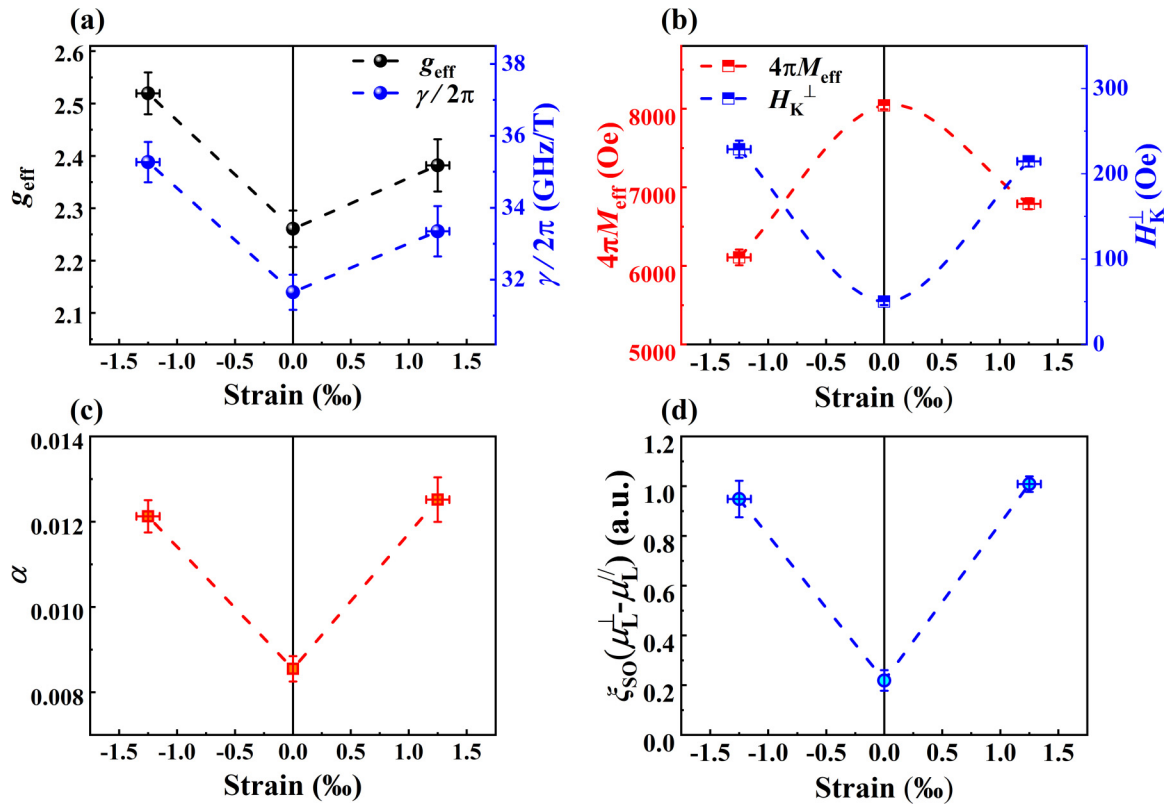


FIG. 6. (a) Calculated g_{eff} and the refits gyromagnetic ratio $\gamma/2\pi$ as a function of strain. (b) The refit of the extracted value of $4\pi M_{\text{eff}}$, H_{K}^{\perp} using Eq. (2) as a function of the applied strain. (c) The refit Gilbert damping as a function of the applied strain. (d) The refit spin-orbit term as a function of strain.

a strain-free state is 31.6 ± 0.5 , which matches the reported value of 31.4 ± 0.2 [18].

Using the values of γ derived from XMCD measurements, we refit our FMR data. The refitted values of H_{K}^{\perp} , Gilbert damping α , and SOC-related terms $\xi_{\text{SO}}(\mu_{\text{L}}^{\perp} - \mu_{\text{L}}^{\parallel})$ are shown in Figs. 6(b)–6(d), respectively. They are all increased in the strained Py films, consistent with the results shown in Figs. 2(d), 3(b), and 3(d), in which a constant value of γ is utilized.

IV. CONCLUSION

In conclusion, our study presents a successful method for modulating spin-orbit coupling (SOC) in pure Py films by applying strain through flexible substrates. This approach is substantiated by the observed correlation between SOC enhancement and both tensile and compressive strain, evidenced by increased Gilbert damping and enhanced perpendicular magnetic anisotropy in the Py films. Employing XMCD analysis and *ab initio* calculations, we have elucidated the

fundamental mechanism behind this strain-induced SOC augmentation, which is the elevated orbit-to-spin moment ratio arising from the altered lattice field that mitigates the orbital quenching effect in the Py films. These findings offer valuable insights into the modulation of magnetic properties in materials and are particularly advantageous for applications in spintronics and magnetic storage technologies, where precise control of spin-related characteristics is crucial.

ACKNOWLEDGMENTS

This work was sponsored by the National Natural Science Foundation of China (Grant No. 51601093) and the Fundamental Research Funds for the Central Universities (Grant No. 30923010923). Singapore Synchrotron Light Source (SSLS) is acknowledged for the use of beamline. This work was supported by the MAT-PULSE project, part of the French PIA project “Lorraine Université d’Excellence” Reference No. ANR-15-IDEX-04-LUE, and by the PEPR Electronique through the France 2030 government grants EMCOM (ANR-22-PEEL-0009).

- [1] A. Soumyanarayanan, N. Reyren, A. Fert, and C. Panagopoulos, Emergent phenomena induced by spin-orbit coupling at surfaces and interfaces, *Nature (London)* **539**, 509 (2016).
 [2] A. Manchon, H. C. Koo, J. Nitta, S. M. Frolov, and R. A. Duine, New perspectives for rashba spin-orbit coupling, *Nat. Mater.* **14**, 871 (2015).

- [3] A. Manchon, J. Železný, I. M. Miron, T. Jungwirth, J. Sinova, A. Thiaville, K. Garello, and P. Gambardella, Current-induced spin-orbit torques in ferromagnetic and antiferromagnetic systems, *Rev. Mod. Phys.* **91**, 035004 (2019).
 [4] E. Sagasta, Y. Omori, M. Isasa, M. Gradhand, L. E. Hueso, Y. Niimi, Y. C. Otani, and F. Casanova, Tuning the spin Hall effect

- of Pt from the moderately dirty to the superclean regime, *Phys. Rev. B* **94**, 060412(R) (2016).
- [5] Q. L. He, T. L. Hughes, N. P. Armitage, Y. Tokura, and K. L. Wang, Topological spintronics and magnetoelectronics, *Nat. Mater.* **21**, 15 (2022).
- [6] N. H. D. Khang, Y. Ueda, and P. N. Hai, A conductive topological insulator with large spin Hall effect for ultralow power spin-orbit torque switching, *Nat. Mater.* **17**, 808 (2018).
- [7] S. J. Barnett, Magnetization by rotation, *Phys. Rev.* **6**, 239 (1915).
- [8] J. B. Goodenough, Spin-orbit-coupling effects in transition-metal compounds, *Phys. Rev.* **171**, 466 (1968).
- [9] L. Zhu, D. C. Ralph, and R. A. Buhrman, Spin-orbit torques in heavy-metal-ferromagnet bilayers with varying strengths of interfacial spin-orbit coupling, *Phys. Rev. Lett.* **122**, 077201 (2019).
- [10] K. Chen and S. Zhang, Spin pumping in the presence of spin-orbit coupling, *Phys. Rev. Lett.* **114**, 126602 (2015).
- [11] A. Hrabec, F. J. T. Gonçalves, C. S. Spencer, E. Arenholz, A. T. N'Diaye, R. L. Stamps, and C. H. Marrows, Spin-orbit interaction enhancement in permalloy thin films by Pt doping, *Phys. Rev. B* **93**, 014432 (2016).
- [12] T. Jungwirth, Q. Niu, and A. H. MacDonald, Anomalous Hall effect in ferromagnetic semiconductors, *Phys. Rev. Lett.* **88**, 207208 (2002).
- [13] S. N. Panda, S. Mondal, J. Sinha, S. Choudhury, and A. Barman, All-Optical detection of interfacial spin transparency from spin pumping in β -Ta/CoFeB thin films, *Sci. Adv.* **5**, eaav7200 (2019).
- [14] Z. Zhang, E. Liu, X. Lu, W. Zhang, Y. You, G. Xu, Z. Xu, P. K. J. Wong, Y. Wang, B. Liu, X. Yu, J. Wu, Y. Xu, A. T. S. Wee, and F. Xu, Strain-controlled spin wave excitation and Gilbert damping in flexible Co_2FeSi films activated by femtosecond laser pulse, *Adv. Funct. Mater.* **31**, 2007211 (2021).
- [15] E. Liu, T. Fache, D. Cespedes-Berroc, Z. Zhang, S. Petit-Watlot, S. Mangin, F. Xu, and J.-C. Rojas-Sánchez, Strain-enhanced charge-to-spin conversion in Ta/Fe/Pt multilayers grown on flexible mica substrate, *Phys. Rev. Appl.* **12**, 044074 (2019).
- [16] B. T. Thole, P. Carra, F. Sette, and G. van Der Laan, X-Ray circular dichroism as a probe of orbital magnetization, *Phys. Rev. Lett.* **68**, 1943 (1992).
- [17] P. Carra, B. T. Thole, M. Altarelli, and X. Wang, X-ray circular dichroism and local magnetic fields, *Phys. Rev. Lett.* **70**, 694 (1993).
- [18] Y. Yin, F. Pan, M. Ahlberg, M. Ranjbar, P. Dürrenfeld, A. Houshang, M. Haidar, L. Bergqvist, Y. Zhai, R. K. Dumas, A. Delin, and J. Åkerman, Tunable permalloy-based films for magnonic devices, *Phys. Rev. B* **92**, 024427 (2015).
- [19] R. Arias and D. L. Mills, Extrinsic contributions to the ferromagnetic resonance response of ultrathin films, *Phys. Rev. B* **60**, 7395 (1999).
- [20] Y. Zhao, Q. Song, S.-H. Yang, T. Su, W. Yuan, S. S. P. Parkin, J. Shi, and W. Han, Experimental investigation of temperature-dependent Gilbert damping in permalloy thin films, *Sci. Rep.* **6**, 22890 (2016).
- [21] P. Bruno, Tight-binding approach to the orbital magnetic moment and magnetocrystalline anisotropy of transition-metal monolayers, *Phys. Rev. B* **39**, 865 (1989).
- [22] I. S. Elfimov, V. I. Anisimov, and G. A. Sawatzky, Orbital ordering, Jahn-Teller distortion, and anomalous x-ray scattering in manganates, *Phys. Rev. Lett.* **82**, 4264 (1999).
- [23] F. Wilhelm, P. Pouloupoulos, P. Srivastava, H. Wende, M. Farle, K. Baberschke, M. Angelakeris, N. K. Flevaris, W. Grange, J.-P. Kappler, G. Ghiringhelli, and N. B. Brookes, Magnetic anisotropy energy and the anisotropy of the orbital moment of Ni in Ni/Pt multilayers, *Phys. Rev. B* **61**, 8647 (2000).
- [24] G. Kresse and J. Furthmüller, Efficiency of *ab-initio* total energy calculations for metals and semiconductors using a plane-wave basis set, *Comput. Mater. Sci.* **6**, 15 (1996).
- [25] P. E. Blöchl, Projector augmented-wave method, *Phys. Rev. B* **50**, 17953 (1994).
- [26] J. P. Perdew, J. A. Chevary, S. H. Vosko, K. A. Jackson, M. R. Pederson, D. J. Singh, and C. Fiolhais, Atoms, molecules, solids, and surfaces: Applications of the generalized gradient approximation for exchange and correlation, *Phys. Rev. B* **46**, 6671 (1992).
- [27] G. Kresse and D. Joubert, From ultrasoft pseudopotentials to the projector augmented-wave method, *Phys. Rev. B* **59**, 1758 (1999).
- [28] C. Aruta, G. Ghiringhelli, V. Bisogni, L. Braicovich, N. B. Brookes, A. Tebano, and G. Balestrino, Orbital occupation, atomic moments, and magnetic ordering at interfaces of manganese thin films, *Phys. Rev. B* **80**, 014431 (2009).
- [29] K. Gilmore, Y. U. Idzerda, and M. D. Stiles, Identification of the dominant precession-damping mechanism in Fe, Co, and Ni by first-principles calculations, *Phys. Rev. Lett.* **99**, 027204 (2007).
- [30] W. Zhang, P. K. J. Wong, X. Zhou, A. Rath, Z. Huang, H. Wang, S. A. Morton, J. Yuan, L. Zhang, R. Chua, S. Zeng, E. Liu, F. Xu, Ariando, D. H. C. Chua, Y. P. Feng, G. van der Laan, S. J. Pennycook, Y. Zhai, and A. T. S. Wee, Ferromagnet/two-dimensional semiconducting transition-metal dichalcogenide interface with perpendicular magnetic anisotropy, *ACS Nano* **13**, 2253 (2019).
- [31] C. T. Chen, Y. U. Idzerda, H.-J. Lin, N. V. Smith, G. Meigs, E. Chaban, G. H. Ho, E. Pellegrin, and F. Sette, Experimental confirmation of the x-ray magnetic circular dichroism sum rules for iron and cobalt, *Phys. Rev. Lett.* **75**, 152 (1995).
- [32] H. A. Dürr and G. van Der Laan, Magnetic circular X-ray dichroism in transverse geometry: Importance of noncollinear ground state moments, *Phys. Rev. B* **54**, R760 (1996).
- [33] W. Zhang, D. Zhang, P. K. J. Wong, H. Yuan, S. Jiang, G. Van Der Laan, Y. Zhai, and Z. Lu, Selective tuning of Gilbert damping in spin-valve trilayer by insertion of rare-earth nanolayers, *ACS Appl. Mater. Inter.* **7**, 17070 (2015).
- [34] D. Weller, J. Stöhr, R. Nakajima, A. Carl, M. G. Samant, C. Chappert, R. Mégy, P. Beauvillain, P. Veillet, and G. A. Held, Microscopic origin of magnetic anisotropy in Au/Co/Au probed with x-ray magnetic circular dichroism, *Phys. Rev. Lett.* **75**, 3752 (1995).
- [35] T. Koide, H. Miyauchi, J. Okamoto, T. Shidara, A. Fujimori, H. Fukutani, K. Amemiya, H. Takeshita, S. Yuasa, T. Katayama, and Y. Suzuki, Direct determination of interfacial magnetic moments with a magnetic phase transition in Co nanoclusters on Au (111), *Phys. Rev. Lett.* **87**, 257201 (2001).
- [36] I. Galanakis, Orbital magnetism in the half-metallic Heusler alloys, *Phys. Rev. B* **71**, 012413 (2005).

- [37] H. J. Elmers, G. H. Fecher, D. Valdaitsev, S. A. Nepijko, A. Gloskovskii, G. Jakob, G. Schönhense, S. Wurmehl, T. Block, C. Felser, P.-C. Hsu, W.-L. Tsai, and S. Cramm, Element-specific magnetic moments from core-absorption magnetic circular dichroism of the doped Heusler alloy $\text{CoC}_{0.6}\text{Fe}_{0.4}\text{Al}$, *Phys. Rev. B* **67**, 104412 (2003).
- [38] A. J. P. Meyer and G. Asch, Experimental G' and g values of Fe, Co, Ni, and their alloys, *J. Appl. Phys.* **32**, S330 (1961).
- [39] É. D. T. De Lacheisserie, D. Gignoux, and M. Schlenker, editors, *Magnetism: II-Materials and Applications* (Springer, Boston, MA, 2002).